Stem Cells, 2025, **43**, sxaf014
https://doi.org/10.1093/stmcls/sxaf014
Advance access publication 1 April 2025
Original Research

Impact of pro-inflammatory cytokine preconditioning on metabolism and extracellular vesicles in feline mesenchymal stromal cells: a preliminary study

Maria Soltero-Rivera[1,2], Boaz Arzi[1,2,*], Lynda Bourebaba[3], Krzysztof Marycz[1,2]

[1]Department of Surgical and Radiological Sciences, School of Veterinary Medicine, University of California-Davis, Davis, CA, United States
[2]Veterinary Institute for Regenerative Cures, School of Veterinary Medicine, University of California-Davis, Davis, CA, United States
[3]Department of Experimental Biology, Faculty of Biology and Animal Science, Wrocław University of Environmental and Life Sciences, Wrocław, Poland

[*]Corresponding author: Boaz Arzi, DVM, DAVDC, DEVDC, FF-AVDC-OMFS, 1285 Veterinary Sciences Mall, VM3A 2303, Davis, CA 95616, USA (barzi@ucdavis.edu).

Abstract

Background: Extracellular vesicles (EVs) derived from mesenchymal stem cells have shown promise in treating inflammation. This study investigates whether preconditioning feline adipose-derived stem cells (FeASCs) with inflammatory cytokines, specifically IFN-γ and TNF-α, enhances the anti-inflammatory efficacy of MSC-derived EVs.

Objective: We hypothesize that cytokine-primed FeASCs will produce EVs with improved anti-inflammatory properties and that this preconditioning will affect mitochondrial dynamics to enhance EV therapy effectiveness.

Methods: FeASCs were exposed to a TNF-α/IFN-γ combination to mimic a pro-inflammatory milieu favoring ASCs' immunosuppressive phenotype. We analyzed morphological, metabolic, and immunomodulatory characteristics of native and cytokine-primed FeASCs. EVs were assessed for anti-inflammatory and mitochondrial-related markers. We also evaluated mitochondrial function and apoptosis markers in cytokine-primed cells.

Results: Cytokine priming led to significant morphological changes in FeASCs, including enhanced cell projections and increased apoptosis. EVs from cytokine-primed FeASCs exhibited a heightened immunomodulatory profile, with increased expression of both pro-inflammatory and anti-inflammatory mediators. Transcriptomic analysis of these EVs revealed the upregulation of genes associated with cell proliferation, survival, and apoptosis. Mitochondrial function was impaired in cytokine-primed cells, but mitochondrial morphology remained unchanged. EVs from these cells contained higher levels of mitochondrial-related transcripts, indicating a compensatory response.

Conclusions: Cytokine-primed FeASCs generate EVs with enhanced immunomodulatory potential, highlighting their therapeutic promise. However, further research is needed to validate their efficacy and safety and refine preconditioning strategies to optimize EV-based therapies for inflammatory conditions. These advancements could pave the way for broader applications in regenerative medicine.

Key words: extracellular vesicle; feline; regenerative medicine; stromal cell; adipose; placental.

Received: 4 September 2024; Accepted: 14 March 2025.

Graphical Abstract

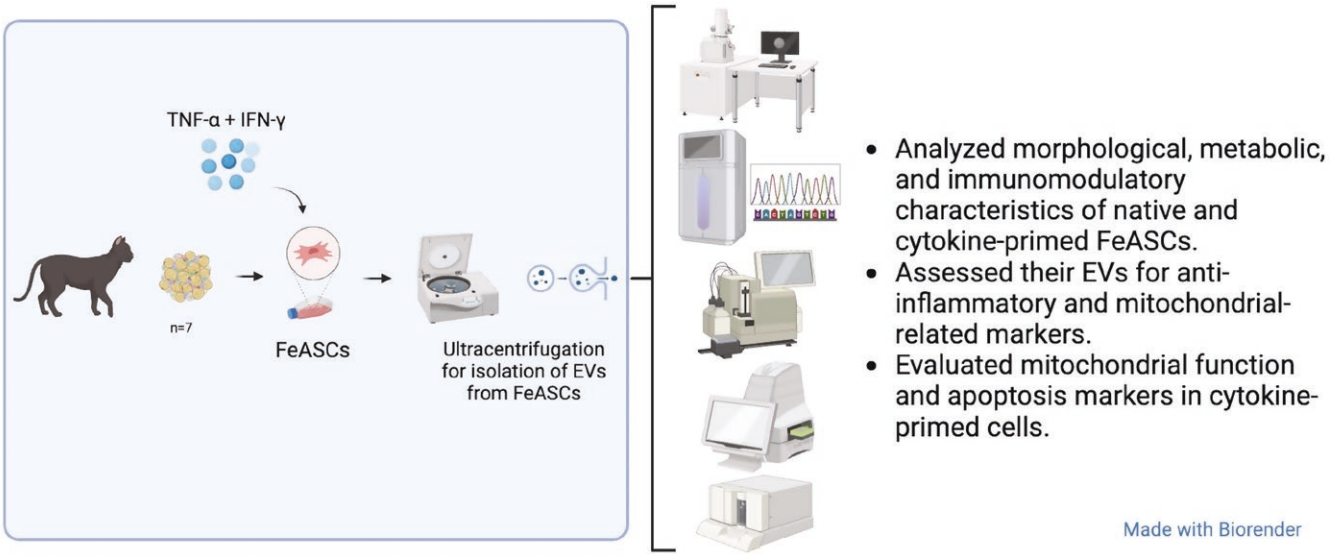

Significance Statement

This study explores an innovative approach to enhancing the therapeutic potential of extracellular vesicles (EVs) derived from feline adipose-derived stem cells (FeASCs) by preconditioning these cells with inflammatory cytokines. Our findings demonstrate that cytokine priming significantly boosts the immunomodulatory properties of FeASC-derived EVs. We have also evaluated alterations in mitochondrial dynamics and cell morphology, suggesting that preconditioning with IFN-γ and TNF-α/IL-1β influences EV composition and modifies cellular processes related to inflammation and cell survival. These findings lay the foundation for enhancing EV-based therapies for inflammatory diseases, with potential applications extending to regenerative medicine and other fields.

Introduction

Mesenchymal Stromal Cells (MSCs) are known in feline regenerative medicine for their pro-regenerative capabilities and significant role in modulating immune responses.[1-5] These cells successfully treated refractory feline chronic gingivostomatitis (FCGS), achieving an approximately 70% response rate.[1-3,5] FCGS shares similarities with human chronic inflammatory and autoimmune diseases, making cats a valuable translational model. Cats with chronic oral inflammation exhibit immune dysregulation, including elevated pro-inflammatory cytokines, similar to human conditions like oral lichen planus and severe periodontal disease.[6,7] Utilizing feline MSCs provides a biologically relevant and clinically translatable approach to developing regenerative treatments for both veterinary and human chronic oral inflammation.

The finding that cell–cell contact was not always required for the immunomodulatory qualities of MSCs led to the discovery of the paracrine agents that stimulate this response. Extracellular vesicles (EVs), including exosomes and microvesicles, are small membrane-bound particles released by cells, including MSCs. These EVs are crucial in intercellular communication, carrying proteins, lipids, and nucleic acids and thereby affecting the behavior of recipient cells. Depending on the cell source, EVs can be either pro-inflammatory or anti-inflammatory. Research on the therapeutic potential of MSCs and their EVs has been on a trajectory, particularly in feline regenerative medicine and treating inflammatory diseases. EVs have the potential to overcome several challenges associated with MSCs, such as immunogenicity, off-target homing, heterogeneity, and difficulties related to storage and handling, thereby improving the scalability and sustainability of this therapeutic approach.[8,9]

Inflammation is a complex and fundamental biological response to harmful stimuli, including pathogens, damaged cells, or irritants. Key cytokines involved in inflammation include tumor necrosis factor-alpha (TNF-α), interleukin-1 beta (IL-1β), and interleukin-6 (IL-6), which play pivotal roles in initiating and sustaining the inflammatory response.[10-16] These cytokines activate signaling pathways like STAT3 and STAT6, crucial for mediating immune responses and maintaining homeostasis. Transforming growth factor-beta (TGF-β) is another essential cytokine that, while typically associated with anti-inflammatory effects, can also play diverse roles depending on the context of the inflammatory environment. Dysregulation of these cytokines and signaling pathways is implicated in various inflammation-related diseases, highlighting the need for effective therapeutic strategies.[11]

Priming MSCs refers to preconditioning these cells to enhance their therapeutic potential before transplantation. Priming involves exposing MSCs to specific stimuli or conditions that induce beneficial changes in their behavior, function, and survival. Priming can significantly improve the effectiveness of MSCs in various therapeutic applications, including tissue regeneration, immunomodulation, and treatment of inflammatory diseases.[17-24] Methods of priming MSCs include cytokine and growth factor priming. Interferon-gamma (IFN-γ) enhances the immunomodulatory properties of MSCs by upregulating the expression of

indoleamine 2,3-dioxygenase (IDO) and other anti-inflammatory molecules.[18] Tumor Necrosis Factor-alpha (TNF-α) and Interleukin-1 beta (IL-1β) promote the secretion of anti-inflammatory and trophic factors, boosting the regenerative and anti-inflammatory potential of MSCs.[25-28]

Mitochondria are highly versatile organelles that quickly adapt to various stressors, playing critical roles in energy conversion, cell death signaling, and the production of reactive oxygen species. Mitochondria can also control inflammation. Numerous studies have demonstrated that transferring mitochondria from MSCs to other cells can influence critical processes, including proliferation, differentiation, metabolism, inflammatory responses, senescence, stress response, and migration.[29-35] A study characterizing the distinctive features of EVs extracted from feline adipose-derived MSCs (ASCs) and placenta-derived MSCs (PMSCs) showed superior CD81 expression in placenta-derived MSCs (PMSCs), indicating their potential as preferred donors of mitochondria. However, differential microRNA expression in EVs derived from ASCs hinted at their superior anti-inflammatory and immunometabolic features (Soltero-Rivera 2024).[36] Preconditioning adipose-derived stromal cells (ASCs) enhance the anti-inflammatory properties of their EVs by modulating mitochondrial kinetics.[37-40] This modulation likely involves mitochondrial fission, fusion, and biogenesis alterations, affecting the mitochondrial metabolic state and the bioactive cargo loaded into EVs.[37-40] Little is known about the outcome of priming feline ASCs (FeASCs) on the continuous processes of mitochondrial fission (division) and fusion, which helps maintain mitochondrial function, energy production, and cell health. This process is otherwise known as mitochondrial dynamics.[41] However, the modulation of mitochondrial kinetics through preconditioning could play a pivotal role in enhancing the anti-inflammatory properties of the EVs they generate.

This study aims to evaluate the effects of cytokine priming on the morphological, metabolic, and immunomodulatory characteristics of feline adipose-derived stem cells (FeASCs) by exposing them to IFN-γ and TNF-α/IL-1β. We seek to determine whether EVs derived from cytokine-primed FeASCs exhibit enhanced anti-inflammatory properties compared to non-primed controls. Additionally, we investigate how cytokine priming influences mitochondrial function, apoptosis, and inflammatory signaling within FeASCs. Lastly, we analyze EVs' mitochondrial and inflammatory transcriptomic profiles to assess their potential role in enhancing therapeutic efficacy for inflammatory conditions. We hypothesize that preconditioning feline adipose-derived stem cells (FeASCs) with inflammatory cytokines (IFN-γ and TNF-α/IL-1β) enhances the therapeutic potential of MSC-derived EVs by modulating mitochondrial kinetics and immunomodulatory properties. If successful, this approach mimics the inflammatory environment seen in FCGS and could potentially optimize EV-based therapies for inflammatory conditions.

Materials and methods

Adipose tissue harvesting, ASCs isolation, and EV's collection

Adipose tissue was collected from 7 healthy cats during sterilization procedures with the written consent of the animals' owners. All study procedures were reviewed and approved by the Environmental and Life Sciences University, Wroclaw, Poland. All owners consented to sample acquisition before collection. All procedures for tissue isolation were performed under sterile conditions using an enzymatic-mechanical method. Tissue specimens were washed 3 times in sterile phosphate-buffered saline (PBS) with a 1% penicillin-streptomycin (PS) antibiotic solution (Biowest, USA). The adipose tissue was then fragmented using a surgical scalpel and incubated in a 0.1 mg/mL collagenase type I solution (Sigma-Aldrich, Poland) for 40 minutes at 37 °C and 5% CO_2. Dissociated tissue fragments were afterward filtered using a 70 µm tissue strainer, centrifuged at 1200 × *g* for 10 minutes, and washed twice with PBS. The isolated ASCs were cultured in Dulbecco's Modified Eagle's Medium (DMEM) with 1 g/L glucose, supplemented with 10% fetal bovine serum (FBS) and 1% PS antibiotic solution. ASC cultures were maintained in a humidified CO_2 incubator (37 °C, 5% CO2, 95% air atmosphere) and harvested every 3 days (80%-90% of confluence) using a trypsin-EDTA solution (Sigma-Aldrich, Poland).

EVs were isolated from adipose-derived stem cells (ASCs) following the methodology previously described by our group.[9] The cells were cultured in standard conditions in low glucose Dulbecco's modified eagle's medium (LG-DMEM) supplemented with 10% FBS and 1% PS until they reached approximately 80% confluence. Before EVs isolation, the cells were washed twice with PBS and cultured in serum-free DMEM supplemented with 1% insulin-transferrin-selenium (ThermoFisher Scientific) for 48 hours to avoid contamination with serum-derived EVs. The conditioned medium was collected after 72 hours and filtered 3 times using a 0.22 µm filter to remove cell debris and larger particles. The supernatant was centrifugated at 300 × *g* at 4 °C for 10 minutes to remove cell debris. The obtained supernatant was transferred to a new Eppendorf tube and centrifuged at 21 000 × *g* for 1 hour to pellet the EVs. As previously described, the final EVs pellet was resuspended in sterile PBS and stored at −80 °C for further analysis.

Priming of ASCs using cytokine cocktail

To induce inflammatory priming, ASCs were cultured until they reached approximately 80% confluence in Dulbecco's modified eagle's medium (DMEM) supplemented with 10% FBS and 1% PS. Thereafter, the complete culture medium was replaced with fresh FBS-free DMEM supplemented with 1% insulin-transferrin-selenium, 15 ng/mL TNF-α (Sigma-Aldrich, Poland), and 10 ng/mL IFN-γ (Sigma-Aldrich, Poland), and cultures incubated during 72 hours in a humidified CO_2 incubator. This pretreatment aimed to stimulate the cells and enhance their immunomodulatory properties.[42,43] Following the priming period, the cell's supernatant was recovered for EV isolation, as described in the previous section.[44]

EVs surface and size analysis

Detailed morphological analysis of EVs was performed using scanning electron microscopy (SEM; Zeiss EVO LS15). Isolated EVs were first adsorbed onto poly-L-Lysin-coated glass coverslips for 1 hour in a humidified chamber and fixed with 2.5% glutaraldehyde (Sigma-Aldrich, Poland) in PBS for 15 minutes. After washing twice with PBS, the fixed EVs were dehydrated with an ascending sequence of ethanol (50%-100%). After evaporation of ethanol, the samples were left to dry at room temperature for 24 hours, sputtered with

gold-palladium (ScanCoat 6, Oxford), and captured using an SE1 detector at 10 kV filament tension. Additionally, the size distribution of the EVs was determined by analyzing SEM images to assess the range of diameters and morphological heterogeneity.[45]

ASCs morphology and ultrastructure

Cell morphology was evaluated using an inverted light microscope for general structural observations, a confocal laser scanning microscope for high-resolution and ultrastructural imaging, and SEM for detailed surface characterization. For general cell morphology assessment, cells were cultured under defined conditions (described above) and observed under an inverted light microscope equipped with a brightfield illumination system (AxioObserverA1; Zeiss) to examine their shape, adherence, and overall structural organization in the culture dish. For detailed cell morphology analysis, ASCs were seeded onto glass coverslips, subjected to each defined culture condition, fixed in cold 4% PFA for 40 minutes at room temperature, and then permeabilized with a 0.1% Triton X-100 solution (Sigma-Aldrich, Poland) for 15 minutes to stain the cytoskeleton. Actin filaments were stained with atto-488-labeled phalloidin (Sigma-Aldrich, Poland) at a concentration of 1:800 in PBS for 45 minutes in the dark at room temperature. Nuclei were counterstained with diamidino-2-phenylindole (DAPI) using the Fluoroshield™ with DAPI mounting medium (Sigma-Aldrich, Poland). To investigate the mitochondrial network, MitoRed dye (Sigma-Aldrich, Poland) was added to the culture medium at a ratio of 1:1000 and incubated for 30 minutes at 37 °C. The excess MitoRed dye was removed by washing with PBS before fixing the cells in 4% PFA for 40 minutes at room temperature in the dark. Coverslips were then mounted onto microscope slides using the Fluoroshield™ with DAPI mounting medium (Sigma-Aldrich, Poland). Stained cells were observed and imaged using a confocal microscope (Observer Z1 Confocal Spinning Disc V.2 Zeiss with live imaging chamber). Obtained photomicrographs were merged and analyzed using *ImageJ* software (Bethesda, MD, USA). The analysis of mitochondrial morphological subtypes was conducted using the MicroP software (version 1.1.11b, Biomedical Image Informatics Lab, Taipei City, Taiwan, affiliated with the National Yang-Ming Chiao Tung University Institute of Biomedical Informatics) integrated with MATLAB (version R2010b, The MathWorks, Natick, MA, USA).[46]

SEM (Zeiss EVO LS15) and focused ion beam (Zeiss, Cobra, AURIGA 60) were utilized for detailed surface morphology analysis. After fixation of cell cultures in 4% PFA overnight at 4 °C, cells were washed with PBS 3 times, dehydrated in graded ethanol solutions (50%-100%), air-dried for 30 minutes at room temperature, and coated with a thin gold layer using a sputter coater (ScanCoat 6, Oxford). Surface images were acquired using a secondary electron (SE1) detector at a filament tension of 10 kV.

RNA extraction

Total RNA was extracted from both cells and EVs using the EXTRAzol reagent (Blirt, Poland), following the manufacturer's protocol. RNA quality and quantity were evaluated using a Bioanalyzer (Agilent Technologies) to ensure RNA Integrity with RINs above 7.0. To maintain biological replicates, 3 separate RNA extractions were performed for each group (control ASCs, cytokine-primed FeASCs, control EVs, and cytokine-primed EVs).

Library preparation and RNA sequencing

RNA libraries were prepared using the Illumina TruSeq RNA Sample Preparation Kit according to the manufacturer's guidelines. Briefly, RNA samples underwent poly(A) enrichment or rRNA depletion, were fragmented, and then reverse-transcribed into cDNA. The cDNA was ligated with sequencing adapters and amplified through PCR. Library quality was assessed with a nano spectrophotometer (Epoch, BioTek), and sequencing was conducted on the Illumina NovaSeqX (Illumina, San Diego, CA) platform, generating paired-end reads of 100 bp.

Data analysis

Raw sequencing data were processed with HTStream (https://s4hts.github.io/HTStream/). Reads were aligned to the cat reference genome (felCat9.2_X; GCA_000181335.6) using the STAR aligner. Differential expression analysis was conducted using DESeq2, with transcript quantification to evaluate gene expression changes between control and primed FeASCs and their respective EVs.

The RNASeq library preparation followed a straightforward, strand-specific protocol combining the Illumina TruSeq RNA method with dUTP techniques.

Gene expression and miRNA analysis

cDNA was synthesized from RNA collected from control FeASC, primed FeASCs, and their EVs utilizing the Takara PrimeScript™ RT Reagent Kit with gDNA Eraser (Perfect Real Time; Takara, Japan), following the manufacturer's instructions. Quantitative real-time polymerase chain reaction (qPCR) was performed using the SensiFast SYBR & Fluorescein Kit (Bioline, London, UK) and the CFX Connect™ Real-Time PCR Detection System (Bio-Rad, Poland). Each reaction included 150 ng of cDNA in a final volume of 10 µL. The thermal cycling conditions were set as follows: an initial denaturation at 95 °C for 2 minutes, followed by 41 cycles of denaturation at 95 °C for 15 seconds, annealing for 30 seconds, and elongation at 72 °C for 15 seconds. The RT-qPCR reactions were conducted in triplicate. Relative gene expression levels were normalized to glyceraldehyde 3-phosphate dehydrogenase (GAPDH) using the $2^{-\Delta\Delta Cq}$ method.

The Mir-X miRNA First-Strand Synthesis Kit (Takara, Sweden) was utilized to perform RT-qPCR for miRNA. Briefly, genomic DNA (gDNA) traces were eliminated by treating RNA with DNase I, RNase-free, in a 10× reaction buffer containing MgCl2 and water at 37 °C for 30 minutes. The obtained RNA (1000 ng/µL) was then mixed with mRQ Buffer (2X) and mRQ Enzyme. The reaction mixture was incubated at 37 °C for 1 hour and 85 °C for 5 minutes. The expression levels of miRNA were analyzed using Real-Time PCR with the microRNA First-Strand Synthesis Kit (Takara, Sweden), following the manufacturer's instructions. The reaction mixture included water, SensiFast SYBR & Fluorescein Kit (Bioline, London, UK), miRNA-specific primer, mRQ 3′ primer, and cDNA. U6F and U6R primers were used as reference samples. The

relative expression levels were calculated by comparing the tested groups with the control group using the $2^{-\Delta\Delta Cq}$ method (Livak & Schmittgen, 2001).

Microcapillary cytometry

Cell metabolism was assessed using microcapillary cytometry with the Muse™ Cell Analyzer (Merck Millipore, Darmstadt, Germany) in control FeASCs and primed FeASCs.

Cell viability was examined using the Muse® Count & Viability kit t (Merck Millipore, Darmstadt, Germany). Cultured cells were suspended in 20 µL of assay buffer and incubated with 380 µL of the Muse® Annexin V and Dead Cell reagent at room temperature for 5 minutes. Then, these were analyzed with the Muse™ Cell Analyzer (Merck Millipore, Darmstadt, Germany) to monitor the number of cells distributed across: (i) Live cells: Intact membrane, no uptake of the dye, showing low/no fluorescence intensity. (ii) Dead cells: The membrane is compromised, and the dye penetrates, showing high fluorescence intensity.

The activation of total cellular caspases 1, 3, 4, 5, 6, 7, 8, and 9 were analyzed using the Muse MultiCaspase assay kit (Merck Millipore, Darmstadt, Germany) in accordance with the provided protocol. Native and cytokine-primed cells were stained with 5 µL of the Muse™ multicaspase reagent working solution and incubated for 30 minutes at 37 °C. Next, 150 µL of the Muse™ caspase 7-amino actinomycin D (7AAD) working solution was added, and the samples were incubated for 5 minutes in the dark at room temperature. The levels of multicaspase activity were subsequently measured using the Muse Cell Analyzer (Merck Millipore, Darmstadt, Germany).

The Muse MitoPotential analysis was performed to analyze mitochondrial transmembrane potential. Briefly, 90 µL of MitoPotential Working Solution (1:1000 in 1 × Assay Buffer; Merck Millipore, Darmstadt, Germany) was mixed with 100 µL of cells and incubated at 37 °C for 20 minutes. Subsequently, 5 µL of Muse®-7AAD reagent (Luminex, Poland) was added. After a 5-minute incubation at room temperature in the dark, the mitochondrial potential was assessed using the Muse™ Cell Analyzer (Merck Millipore, Darmstadt, Germany) equipped with Muse™ Software.

Microscopic evaluation of ASC cell viability

Live/dead staining was performed using Calcein-AM/Propidium Iodide (PI; Sigma-Aldrich, Poland) assay to distinguish live from dead populations. Cells seeded onto glass coverslips were incubated with 2 µM Calcein-AM (Invitrogen, Poland) and 1 µg/mL PI in PBS for 30 minutes at 37 °C. After incubation, cells were washed 3 times with PBS to remove any unbound dye. Coverslips were then mounted onto microscope slides using Fluoroshield™ histology mounting medium (Sigma-Aldrich, Poland). The fluorescence signals were observed and imaged using a confocal microscope (Observer Z1 Confocal Spinning Disc V.2 Zeiss with live imaging chamber) at 400× magnification. Obtained images were merged and analyzed using *ImageJ* software (Bethesda, MD, USA).

Comprehensive analysis of mitochondrial and glycolytic function in ASCs using the seahorse XF analyzer

The Seahorse XF Analyzer was employed to evaluate various aspects of cellular metabolism, including oxygen consumption rate (OCR) kinetics, extracellular acidification rate (ECAR) kinetics, mitochondrial respiration profile, and glycolytic function in control FeASCs and cytokine-primed FeASCs. The OCR technique has been applied to measure real-time mitochondrial respiration kinetics. The experiment involved sequential injections of specific compounds: oligomycin (1 µM; Sigma-Aldrich, St. Louis, MO, USA), FCCP (1 µM; Sigma-Aldrich), a mix of rotenone (1 µM; Sigma-Aldrich) and antimycin A (1 µM; Sigma-Aldrich), and spare respiratory capacity.

The ECAR kinetics were used to measure the glycolytic activity of ASCs. ECAR kinetics involves monitoring the acidification of the extracellular environment, primarily due to lactate production during glycolysis. Real-time OCR measurements were obtained following sequential injections of oligomycin (1 µM; Sigma-Aldrich, St. Louis, MO, USA), FCCP (1 µM; Sigma-Aldrich), and a combination of rotenone (1 µM; Sigma-Aldrich) and antimycin A (1 µM; Sigma-Aldrich). These injections allowed the calculation of basal respiration, ATP-linked respiration, maximal respiration, and spare respiratory capacity.

The mitochondrial respiration profile of control FeASCs and cytokine-primed FeASCs offered a detailed examination of mitochondrial function under normal and stressed conditions. This profile was derived from OCR kinetics data, including basal respiration (indicating energy demand under standard conditions), proton leak (reflecting the integrity of the inner mitochondrial membrane), and non-mitochondrial respiration (representing oxygen consumption not associated with the mitochondrial electron transport chain). Reagents used include oligomycin (1 µM; Sigma-Aldrich, St. Louis, MO, USA), FCCP (1 µM; Sigma-Aldrich), rotenone (1 µM; Sigma-Aldrich), and antimycin A (1 µM; Sigma-Aldrich). The glycolytic function was measured using the ECAR technique, providing data regarding the cells' glycolytic rate, capacity, and reserve. The assay involved the use of glucose (10 mM; Sigma-Aldrich), oligomycin (1 µM; Sigma-Aldrich), and 2-deoxyglucose (50 mM; Sigma-Aldrich).

Multiplex cytokine profiling analysis of EVs payload

The levels of various cytokines and growth factors, including FAS, Fit-3L, GM-CSF, IFN-γ, IL-1β, IL-2, PDGF-BB, IL-12P40, IL-13, IL-4, IL-6, IL-8, KC, SDF-1, RANTES, SCF, MCP-1, TNF-α, and IL-18, were measured using a multiplex Luminex platform with the 16 Multi-Plex Kit (Millipore, Saint Charles, MO). In brief, beads conjugated with analyte-specific antibodies were incubated overnight at 4 °C on an orbital shaker, along with 25 µL of assay buffer, 25 µL of X-Vivo 15, and 25 µL of the sample in the dark. The next day, the plate was allowed to reach room temperature, and the fluid was aspirated using a vacuum manifold. After washing, 25 µL of detection antibodies were added to each well and incubated for 1 hour at room temperature on the orbital shaker. Following this, 25 µL of Streptavidin-Phycoerythrin was added to each well, and incubation continued for 30 minutes at room temperature on a plate shaker. The plate was washed 3 times, and 150 µL of 1× Sheath fluid (Bio-Rad Laboratories Inc, Hercules, CA) was added to each well. Fluorescence was then measured using a Bio-Plex 200 System (Bio-Rad Laboratories Inc, Hercules, CA), and the data were analyzed with Bio-Plex Manager software (Bio-Rad

Laboratories) using a 5-parameter model to determine final concentrations (expressed in pg/mL). Reference samples were included on each plate to ensure assay consistency.

Statistical analysis

Data were analyzed by one-way analysis of variance (ANOVA) using GraphPad Software 8 (San Diego, USA) followed by post hoc Tukey's test. Statistically significant results were indicated with an Asterix: $P < .05$ (*), $P < .01$ (**), $P < .001$ (***), and $P < .001$ (****) when comparing native to cytokines-primed groups of either FeASCs or EVs. Results are presented as the mean ± SD from at least 3 independent experiments, each with 3 technical replicates.

Results

Impact of cytokines conditioning on FeASCs morphological and metabolic characteristics

MSCs' morphological changes are vital indicators of their functionality and differentiation potential, providing essential insights into their ability to contribute to tissue regeneration and repair. Therefore, morphological characteristics of FeASCs cultured under standard and priming conditions were analyzed using confocal scanning fluorescent and electron microscopy.

As shown in Figure 1A, feline ASCs cultured under standard conditions exhibited typical stellate morphology, characterized by the presence of multiple cytoplasmic processes radiating from the cellular body, resembling a starburst pattern, which is consistent with their inherent fibroblastic nature, allowing them to extend processes as they adhere to the culture substrate and interact with the culture environment. Moreover, SEM micrographs revealed the presence of multiple prominent nucleoli, suggesting an intensified transcriptional activity of the cells (Figure 1A). Interestingly, FeASCs cultured in the presence of the TNF-α/IFN-γ cytokines cocktail displayed enhanced cytoplasmic and membrane projections made of filipodia and lamellipodia and increased cell spreading and size, indicating the establishment of an adaptive mechanism to the priming milieu. Similarly to native ASCs, the cytokine-primed cells were characterized by more prominent nucleoli, signing the cells' increased nuclear activity.

The observation of EVs isolated from both native and cytokine-primed FeASCs-derived culture media under a scanning electron microscope showed the existence of several spherical EVs displaying surface protrusions and irregularities (Figure 1B). The EVs from both groups were characterized by their heterogeneous appearance, with relative sizes ranging from 300 nm to 500 nm (Figure 1C). However, the cytokine-primed EVs display a greater degree of heterogeneity compared to their native counterparts, with some vesicles reaching an average size of 600 nm. Though not statistically significant, this increased diversity in size could be due to priming influencing the biogenesis and composition of these vesicles.

Cultures were tested for viability and apoptosis rates to investigate further the impact of pro-inflammatory cytokines preconditioning on cellular metabolic activity. Native ASCs presented positive fluorescence exclusively for Calcein-AM, indicating intact cell membranes and metabolically active cells (Figure 1D). In contrast, cytokine-primed FeASCs displayed positive PI staining, suggesting compromised membrane integrity in cellular subsets, highlighting early apoptotic changes or increased cellular stress under priming conditions (Figure 1D). These observations have been subsequently confirmed by the flow cytometric discrimination of total living and dead cells, where cells exposed to cytokines combination presented a significantly higher ($P < .001$) proportion of dead cells compared to unprimed cells (Figure 1F). The apoptotic tendency of cytokine-primed cells has been additionally found to correlate with notable higher PAN caspase activation, in opposition to cells cultured under standard conditions ($P < .001$), implying the initiation of programmed cell death in primed cells (Figure 1H). Furthermore, RT-qPCR data underscored a marked overexpression of master apoptosis regulators, including p53 and p21, in comparison to untreated ASCs ($P < .001$), confirming an increased apoptotic signaling in cytokine-primed cells (Figure 1I).

RNA sequencing was performed on EVs from both cell groups to identify transcripts related to proliferation and apoptosis. As illustrated in Figure 1J, EVs derived from TNF-α/IFN-γ-exposed ASCs were found to cargo higher levels of essential transcripts modulating cell proliferation and cell cycle PIK3CA, JAK2, CCND1, PCNA, suggesting that these EVs may promote cell growth, proliferation, and survival, being further confirmed by the observed a 1.7-fold higher level of the pro-survival BCL2 mRNA in the same group of EVs (Figure 1K). Interestingly, elevated expressions of CASP10 and TP53 mRNAs were identified in the EVs isolated from cytokine-primed FeASCs, highlighting the possible ability of these EVs to regulate cell proliferation through balanced apoptotic signals and genomic stability mechanisms (Figure 1K).

Distinct inflammatory profile of FeASCs and derived EVs under native and cytokines-primed conditions

In order to evaluate the variations in the expression of inflammatory mediators in EVs isolated from FeASCs cultured under standard and priming conditions, transcript levels of selected markers were determined using the RT-qPCR technique. As shown in Figure 2A, EVs isolated from native FeASCs displayed lower levels of IL-8 ($P < .0001$), TNFA ($P < .05$), IL1B ($P < .01$), and STAT3 ($P < .0001$) pro-inflammatory markers compared to their originating cells. At the same time, the expression of IFNG was higher in the same group of EVs ($P < .05$). Interestingly, only IL-8, IL-6, and STAT3 mRNAs were found at lower levels in EVs deriving from cytokine-primed FeASCs, while both TNFA and IL1B transcripts were detected at higher rates ($P < .0001$). The analysis of anti-inflammatory genes (Figure 2B) revealed that native EVs cargo increased levels of IDO1 ($P < .0001$), IL-10 ($P < .0001$), IL-13 ($P < .0001$), IL-4 ($P < .0001$), TGFB ($P < .0001$), and STAT6 ($P < .05$), whereas low expression of EphA2 has further been observed ($P < .0001$). A similar tendency was observed for EVs isolated from TNF-α/IFN-γ-primed FeASCs for IL-10 ($P < .0001$), TGFB ($P < .0001$), and IL-4 ($P < .0001$). In contrast, IL-13 ($P < .0001$) and STAT6 ($P < .0001$) transcripts were significantly downregulated in comparison to cytokine-primed FeASCs (Figure 2B). Notably, no statistical difference in EphA2 expression was noted between cytokine-primed FeASCs and their derived EVs, yet IDO1 mRNA was not detected in both group.

An RNA sequencing approach has been undertaken to analyze further the priming microenvironment's impact on EV

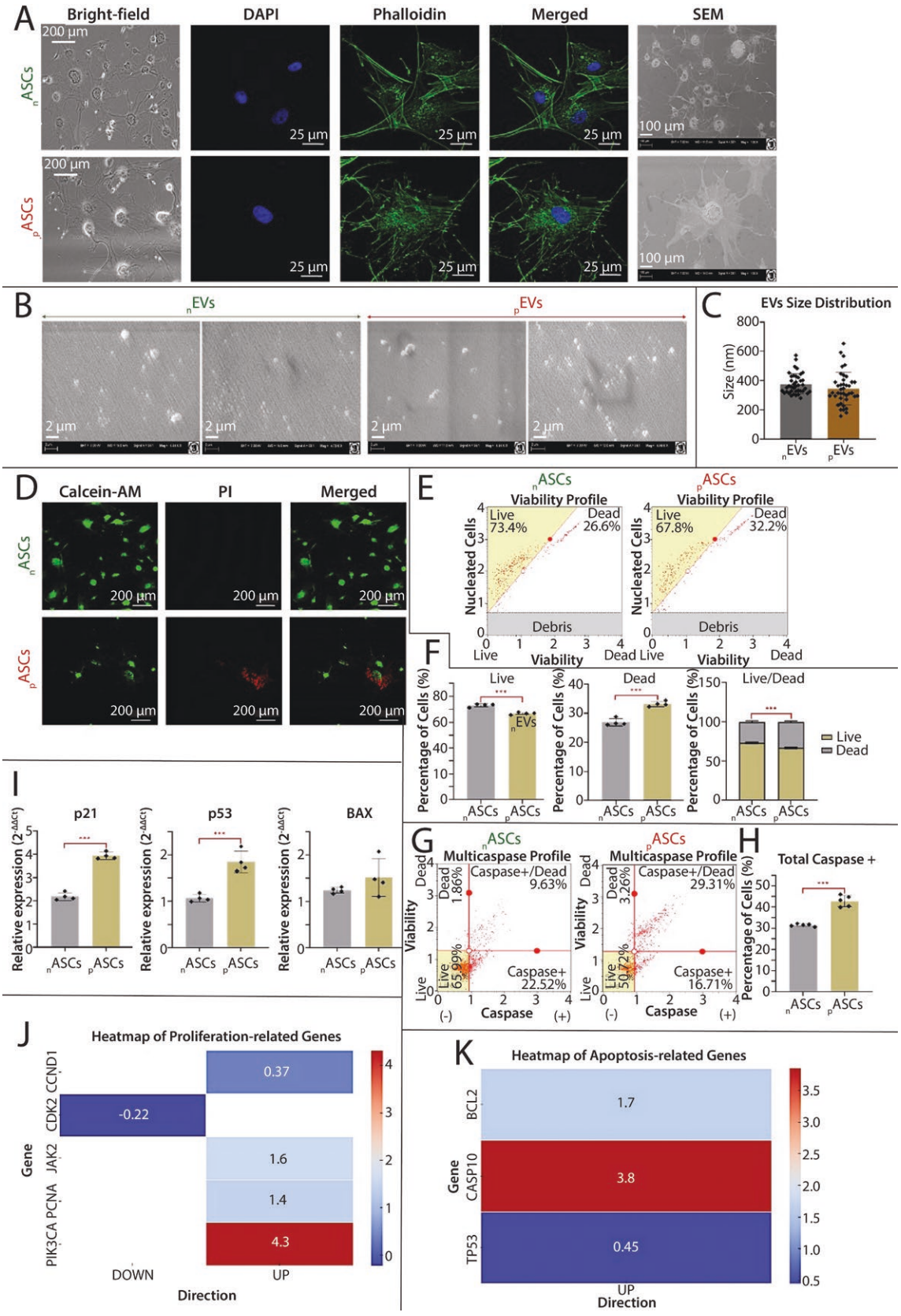

Figure 1. Morphological and functional characterization of feline ASCs under standard and TNF-α/IFN-γ priming conditions. (A) Typical morphology of native and cytokine-primed FeASCs observed under a bright field, a confocal laser scanning fluorescent, and electron microscopes. (B) SEM micrographs of EVs released by ASCs cultured under standard and priming conditions. (C) The average EV size distribution was determined using SEM analysis. (D) Viability assessment using Calcein-AM and PI staining. (E) Representative dot plots for cell count and viability assay. (F) Microcapillary flow cytometric analysis of living and dead cells in native and cytokine-primed FeASCs. (G) Representative density plot for caspase activation profile (H) PAN caspase activation levels in native and cytokine-primed cells. (I) Relative gene expression of proapoptotic genes. (J) RNA sequencing heatmap of proliferation-related transcripts in TNF-α/IFN-γ-treated ASCs-derived EVs versus native EVs. (K) Transcriptome data map for mRNA levels of markers involved in apoptosis regulation detected in cytokine-primed EVs versus native EVs. Representative data is shown as mean ± SD. $_n$ASCs, native

inflammatory payload. Exposure of FeASCs to a TNF-α/IFN-γ cocktail resulted in an increased expression of IL-6, IL-23A, NF-κB1, IFNGR, RELA, and CXCL8 pro-inflammatory factors in the shed EVs (Figure 2C). Interestingly similar trends were observed for selected anti-inflammatory mediators including TGFβ1 and its receptor TGFβR1, IL-10RA, IL-13, IL-4. On the other hand, the transcripts sequencing demonstrated a visible downregulation of IL-1β, TNF-α, IL-12A, and CXCL10. Other mediators implicated in pro-inflammatory response pathways were found at higher expression levels in cytokine-primed EVs than native ones; these include IL6ST, TNFRSF1A, STAT1, STAT3, MAPK3, MAPK14, CD274, and CD86. Only CD80 pro-inflammatory and CD28 anti-inflammatory proteins appeared downregulated in EVs exposed to the TNF-α/IFN-γ cocktail (Figure 2D).

In light of the observed changes in gene expression of inflammatory markers, the protein concentration of 19 cytokines was quantitatively analyzed using a bead-based immunoassay method. The EVs isolated from FeASCs cultured under standard conditions were characterized by a comparable level of most of the measured analytes, except for PDGF-BB, IL-8, RANTES, and TNF-α which showed increasing levels following 144 hours of culture (Figure 2E). Conversely, the exposure of FeASCs to the priming cocktail engendered significant changes in the cytokines' levels of deriving EVs' cargo. Mainly, the amount of IL-1β, PDGF-BB, IL-8, IL-6, IL-4, KC, SDF-1, MCP-1, and TNF-α were found to substantially increase after 72 and 144 hours of priming compared to native EVs (Figure 2E). Noteworthy, GM-CSF cytokine expression increased after 24 hours of priming initiation. It decreased to comparable levels with native EVs starting 72 hours of priming. RANTES chemokine was detected at a higher concentration after 144 hours of culture than EVs isolated from unprimed FeASCs.

So far, implicated in regulating key biological processes, including immunomodulation, the expression patterns of selected microRNAs (miRs) in FeASCs and their EVs have been evaluated. EVs isolated from native FeASCs were loaded with high levels of miR-10a-3p ($P < .0001$), miR-17-5p ($P < .0001$), miR-21-5p ($P < .0001$), and miR-146b ($P < .0001$). In contrast, both miR-21-3p ($P < .0001$), miR-146a ($P < .0001$), and MALAT ($P < .0001$) were detected at significantly lower rates compared to the originating FeASCs (Figure 2F). Likewise, TNF-α/IFN-γ-stimulated FeASCs yielded EVs carrying higher levels of miR-10a-3p ($P < .0001$), miR-17-3p ($P < .0001$) and miR-17-5p ($P < .0001$). In contrast, other miRs, including miR-10a-5p ($P < 0.05$), miR-21-3p ($P < .0001$), miR-146a ($P < .0001$), and miR-146b ($P < .0001$) were detected at notably lower abundance. On the other hand, the levels of miR-21-5p and MALAT remained similar in cytokine-primed FeASCs and their generated EVs (Figure 2F).

Influence of cytokines priming on the mitochondrial metabolism of FeASCs

Mitochondria are pivotal for ASCs' immunomodulatory effects, governing energy production and metabolic signaling crucial for immune response modulation. Hence, dynamic changes in cellular energetics were measured using a Seahorse Extracellular Flux Assay to understand how the pro-inflammatory milieu impacts cellular energy production and function. Obtained data revealed that exposure of FeASCs to the TNF-α/IFN-γ cocktail led to a critical loss in the respiratory capacity of cells, as evidenced by the depleted basal respiration ($P < .01$) and ATP production ($P < .05$) rates compared to unprimed cells. In contrast, no differences in maximal respiration capacity were observed (Figure 3A). A comparable profile was noted for glycolytic function, where preconditioned cells exhibited significantly reduced glycolysis capacity ($P < .0001$) and glycolytic reserves ($P < .0001$) by contrast to cells cultured under standard conditions (Figure 3B).

Additional assessment of mitochondrial health showed that ASC priming induced a critical mitochondrial depolarization (Figure 3D), resulting in a significant loss in mitochondrial transmembrane potential about unprimed FeASCs ($P < .05$), which aligns with the observed impaired energy metabolism. Surprisingly, the MitoRed stained mitochondrial network did not display any visible difference between the two groups of cells, which appeared as dense, brightly fluorescent organelles diffusely distributed throughout the cytoplasm (Figure 3E). In addition to that, the morphometric analysis of the stained mitochondria (Figure 3F) provided additional confirmation that no significant differences in mitochondrial network morphology between the 2 groups were detected in terms of total mitochondrial surface area, tubules (twisted, branched and simple) as well as globules (small, large and loops) subtypes.

To uncover the distinct EV profile in cytokines-induced FeASCs molecular response, potential mitochondrial metabolism-associated transcripts were screened in cytokine-primed FeASCs-derived EVs using an RNAseq approach. Twenty gene products related to mitochondrial metabolic activity were detected in both EV populations (Figure 3G). Notably, MT-CO1, MT-CO2, MT-CO3, MT-ND2, MT-ND4, MT-ND5, UQCRC2, COX4I1, SDHA, SDHB, and MT-CYB mRNA encoding for crucial components of the oxidative phosphorylation pathway were among the targets with the significantly highest expression levels in cytokine-primed EVs by opposition to native EVs. Moreover, the same EVs were characterized by a higher contain in primary mitochondrial transcription and translation machinery mediators, including NRF1, TFAM, PPARGC1A, and POLOG, reflecting an adaptive response to increased cytokines-mediated cellular stress and energy demand.

Discussion

Preconditioning strategies may optimize the therapeutic potential of MSC-derived EVs across a range of inflammatory conditions.[47,48] This therapeutic potential may be exerted via different pathways, such as reduced STAT3 expression, increased defensin secretion, and increased angiogenic factors via protease-activated receptor-mediated signaling.[48-50] Our study explores the clinically relevant molecular consequence of exposing FeASCs to pro-inflammatory and stimulating microenvironments in vitro and the subsequent generation of EVs with distinct secretion profiles. Here, we have provided for the first time a comprehensive and critical insight into the morphological, metabolic, and immunomodulatory

FeASCs; $_{p}$ASCs, cytokine-primed FeASCs; $_{n}$EVs, EVs isolated from native ASCs; $_{p}$EVs, EVs isolated from cytokine-primed FeASCs. An asterisk (*) indicates a comparison among AD-MSCs and PD-MSCs. $P < .05$, $^{**}P < .01$, $^{****}P < .0001$.

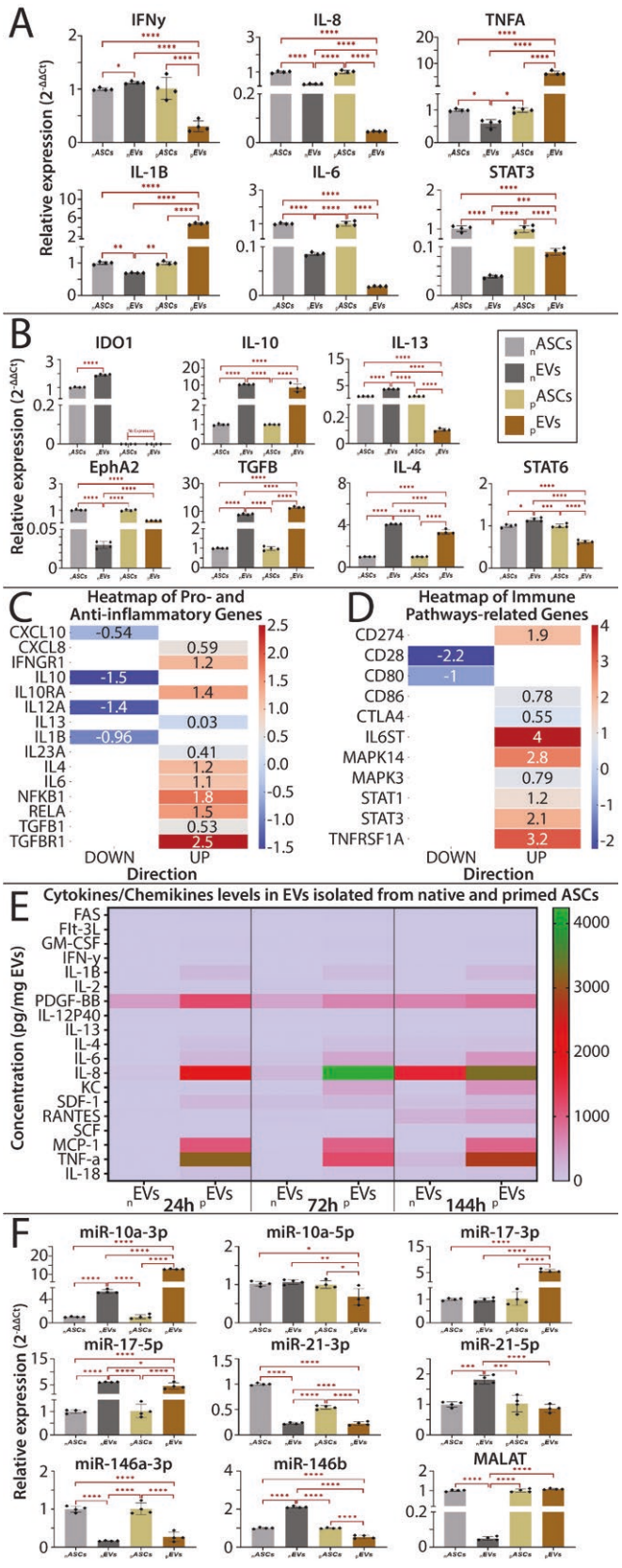

Figure 2. Expression analysis of inflammatory mediators in native and cytokine-primed FeASCs and their derived EVs. (A) Levels of pro-inflammatory markers as measured by RT-qPCR. (B) Expression of anti-inflammatory genes. (C) RNA sequencing results highlighting pro-inflammatory and anti-inflammatory mediator differential levels in EVs from nTNF-α/IFN-γ-primed FeASCs versus native FeASCs EVs. (D) Transcript levels of immune responses associated with modulators were established using the RNAseq approach. (E) Cytokine concentrations in EVs from standard and cytokine-primed FeASCs were analyzed using a bead-based immunoassay. (F) MicroRNA expression profiles in EVs from native and cytokine-primed FeASCs. Representative data is shown as mean ± SD. $_{n}$ASCs, native FeASCs; $_{p}$ASCs, cytokine-primed FeASCs; $_{n}$EVs, EVs isolated from native FeASCs; $_{p}$EVs, EVs isolated from cytokine-primed FeASCs. An asterisk (*) indicates a comparison among AD-MSCs and PD-MSCs. $P < .05$, $^{**}P < .01$, $^{****}P < .0001$.

characteristics of FeASCs and their EVs under native and cytokine-primed conditions, which is essential for future clinical application of EVs in feline veterinary medicine.

Cytokine preconditioning induces morphological changes and apoptotic shifts in FeASCs

We have found that preconditioning of FeASCs with TNF-α/IFN-γ resulted in significant morphological changes, characterized by enhanced cytoplasmic and membrane projections and increased cell spreading.[51-53] These adaptations suggest an activated cellular state, facilitating interaction with the priming environment.[54-56] Electron microscopy revealed prominent nucleoli in native and primed cells, indicating heightened transcriptional activity. However, the primed cells exhibited compromised membrane integrity and increased apoptosis, as evidenced by PI staining and flow cytometry.[57] Cytokine priming of FeASCs led to the induction of apoptosis, as evidenced by the upregulation of proapoptotic genes. Our analysis revealed that the expression of key apoptotic markers was significantly increased, resulting in a slowdown in the proliferation rate of the cells. These findings suggest that prolonged exposure to cytokine stimulation may compromise FeASC viability by shifting the cellular balance toward programmed cell death.

Immonunodulatory and pro-inflammatory properties of EVs

The EVs derived from cytokine-primed FeASCs demonstrated an enhanced ability to modulate inflammatory responses. RNA sequencing of these EVs revealed elevated transcripts associated with cell proliferation, survival, and apoptosis regulation, including PIK3CA, JAK2, CCND1, PCNA, BCL2, CASP10, and TP53. This transcriptomic profile suggests that EVs from cytokine-primed FeASCs can promote cell growth while maintaining a balance between pro-survival and apoptotic signals.

In comparison to native EVs, those from cytokine-primed FeASCs exhibited a distinct inflammatory profile, with higher expression of pro-inflammatory cytokines such as IL-6, IL-8, IL-23A, NF-κB1, TNF-α, IL-1β, and CXCL8 alongside anti-inflammatory mediators like TGFβ1 and IL-10. This selective loading may be an intentional process by the cells to mediate paracrine signaling and amplify the inflammatory response. The timing of EV collection post-stimulation may have influenced these results. The early-phase response might involve upregulation of TNF-α and IL-1β among the first cytokines released during inflammation, whereas other cytokines may be downregulated later. Additionally, the anti-inflammatory effects of EVs from primed FeASCs likely arise from a combination of their cytokine/chemokine cargo and other bioactive molecules, such as microRNAs and lipids, which modulate recipient cell responses. This dual expression pattern may represent an adaptive response for effectively modulating the inflammatory milieu.

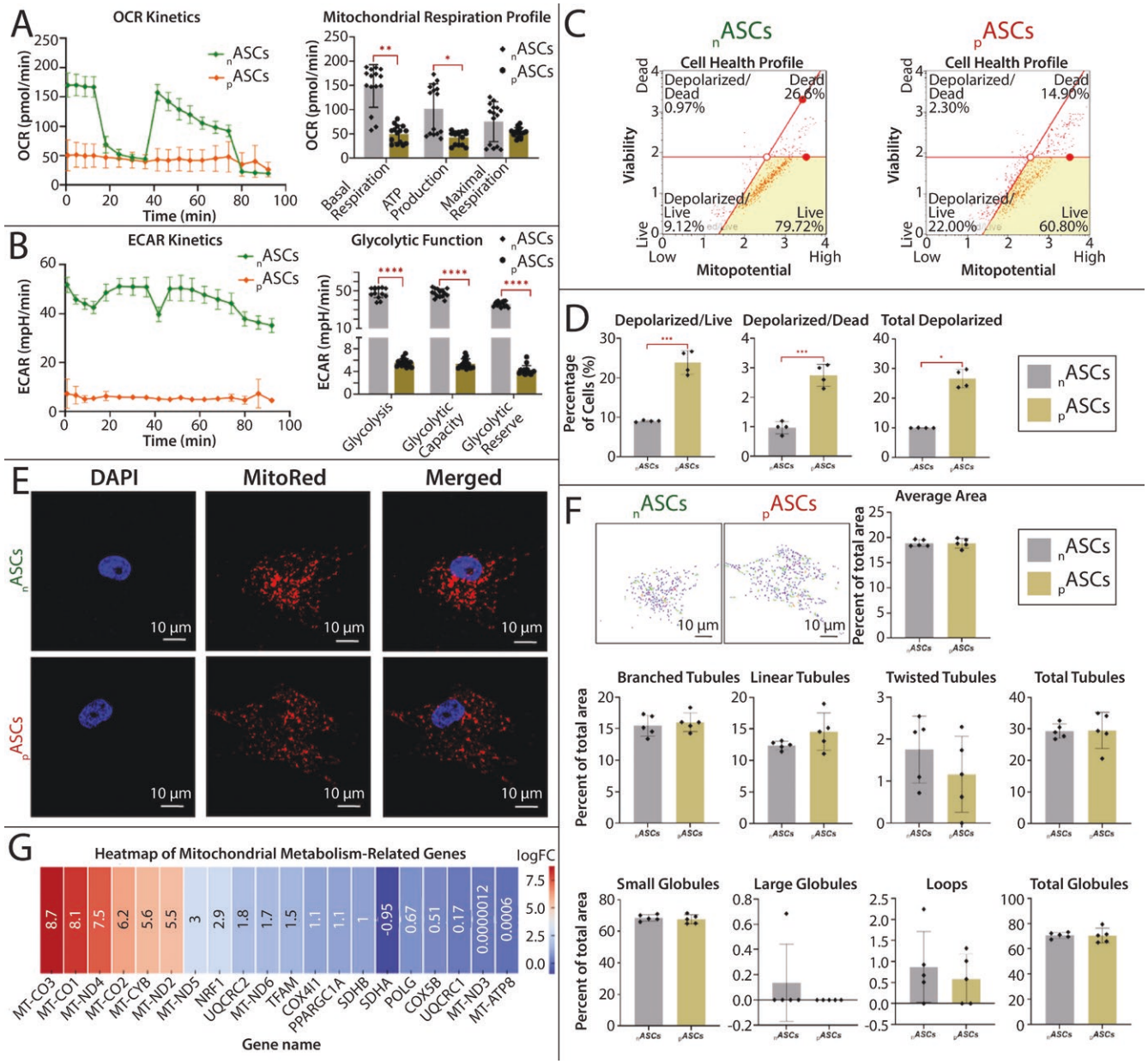

Figure 3. Impact of TNF-α/IFN-γ treatment on FeASCs' mitochondrial metabolism. (A) Oxygen consumption kinetics analysis as an indicator of basal respiration and ATP production rates. (B) Glycolytic capacity and glycolytic reserves determined in native and preconditioned ASCs. (C) representative mitochondrial depolarization Plot (D) Assessment of mitochondrial transmembrane potential. (E) MitoRed-stained mitochondria with DAPI counterstained nuclei were observed under a confocal scanning laser microscope. (F) Morphometric analysis of mitochondria subtypes using MicroP program projection. (G) RNA sequencing of mitochondrial-related gene network associated with biogenesis and metabolism. Representative data is shown as mean ± SD. $_{n}$ASCs, native FeASCs; $_{p}$ASCs, cytokine-primed FeASCs; $_{n}$EVs, EVs isolated from native FeASCs; $_{p}$EVs, EVs isolated from cytokine-primed FeASCs. An asterisk (*) indicates a comparison among AD-MSCs and PD-MSCs. $P < .05$, $^{**}P < .01$, $^{****}P < .0001$.

Impact on mitochondrial metabolism

Mitochondrial dysfunction impairs extracellular vesicle (EV) synthesis by disrupting energy balance, inducing oxidative stress, and altering lipid metabolism. Impaired mitochondrial biogenesis pushes cells into apoptosis, further reducing EV production. Dysfunctional mitochondria not only decrease EV quantity but may also alter their composition, potentially diminishing therapeutic efficacy.[39,58-61]

Our metabolic assessments revealed a significant impact of cytokine priming on FeASCs' mitochondrial function, which may or may not be linked to the transcriptomic changes noted in cytokine-primed FeASCs and their corresponding EVs. Cytokine-primed cells showed decreased respiratory capacity and glycolytic function compared to naïve cells, indicating impaired energy metabolism due to priming. Despite these functional deficits, there were no significant differences in mitochondrial morphology between the 2 groups, suggesting that functional rather than structural alterations drive the observed metabolic changes. These observations align with previous findings that highlight the role of mitochondrial dynamics in cellular adaptation to stress conditions.[62] The preconditioned FeASCs displayed a marked increase in apoptotic markers, including PAN caspases and overexpression of p53 and p21, suggesting the activation of programmed cell

death pathways.[63,64] These results emphasize the delicate balance between cellular activation and stress-induced apoptosis in the context of cytokine priming.

Cytokine-regulated genes in EVs from FeASCs are primarily associated with mitochondrial metabolism and oxidative phosphorylation pathways. RNA sequencing analysis revealed that cytokine-primed FeASC-derived EVs exhibited a significantly higher expression of key mitochondrial genes than EVs from native FeASCs. Among these, MT-CO1, MT-CO2, MT-CO3, MT-ND2, MT-ND4, MT-ND5, UQCRC2, COX4I1, SDHA, SDHB, and MT-CYB were prominently upregulated, indicating an enhanced mitochondrial metabolic activity.[65-69] Additionally, cytokine-primed EVs contained higher levels of NRF1, TFAM, PPARGC1A, and POLOG, which are crucial regulators of mitochondrial transcription and translation.[70-74] This suggests an adaptive response of FeASCs to cytokine-induced stress, leading to increased energy demand and mitochondrial biogenesis, reflected in their EVs' molecular cargo.

Potential clinical impact of EVs with enhanced immunomodulatory properties

In over a decade, there has been a substantial clinical and public interest in regenerative solutions for various disorders in which conventional medicine has failed to provide curative solutions.[75] Cell-based therapies have been used in feline clinical trials for disorders such as chronic kidney disease, chronic enteropathy, and chronic gingivostomatitis (FCGS), to mention a few, and with outcomes supporting MSCs and MSC products as promising therapies.[76,77] Specifically for chronic inflammatory disorders such as refractory FCGS, cats treated with adipose-derived MSCs exhibited substantial improvement or complete durable cure in most cats.[2,3] In a recent retrospective study, an overall positive response rate of 65.5% was noted for refractory cats treated with systemic administration of MSCs, with 58.6% exhibiting long-lasting improvement or complete cure.[4] In that long-term retrospective study, 91% of clients reported seeking treatment with MSCs again if given the opportunity.[4] This clinical response was primarily attributed to immune modulation demonstrated by a significant decrease in the quantity of circulating cytotoxic T cells, normalization of CD4/CD8 lymphocyte rations, and a decrease in circulating neutrophils that corresponded with the positive clinical response.[3] Given that diseases such as FCGS have systemic inflammatory components characterized by increased systemic IFN-γ concentration, allogeneic MSCs may be identified as non-self and eliminated by natural killer cells (NK) upon upregulation of MHC-I induced by IFN-γ.[78] Systemically administered EVs, derived from MSCs rather than MSCs, are likely to circumvent this issue and result in a higher positive response rate.

The authors acknowledge the absence of functional studies, such as in vitro co-culture assays or in vivo transplantation, to confirm whether primed FeASCs or their EVs exhibit enhanced anti-inflammatory properties. While transcriptomic analysis provides insight into how priming influences FeASC activity and EV composition, it does not fully capture the functional impact on target cells. Further evaluation should incorporate transcriptomic and proteomic analyses alongside functional assays to establish a direct link between EV cargo and anti-inflammatory effects. Additionally, the relationship between mitochondrial kinetics and these observed changes remains unverified, as no supporting data are presented. Although both processes are occurring, their connection is uncertain, necessitating targeted blocking experiments to determine causality.

Another consideration is that while cytokine-primed FeASCs may exhibit enhanced immunomodulatory effects, the associated risk of cell damage, reduced viability, immunogenicity, and scarcity of data regarding their long-term effects is a concern.[22,79] Though recent data in mice may contradict these concerns, non-stimulated MSCs may provide a safer, more stable option but may lack the potency needed for severe inflammation.[80,81] An alternative to this would be using EVs from cytokine-primed FeASCs, with a balanced strategy, to help maximize therapeutic efficacy while minimizing risks. Further studies evaluating better priming strategies (ie, milder priming, shorter-duration priming, priming EVs instead of MSCs), different time points after priming, and validating protocols that will improve the safety profile are warranted in order to determine if these findings can be clinically translated.

Conclusion

In summary, cytokine conditioning of FeASCs significantly alters their morphological, metabolic, and immunomodulatory characteristics, resulting in the generation of EVs with enhanced anti-inflammatory properties. These findings underscore the potential of preconditioned FeASCs as a valuable source of therapeutic EVs for modulating inflammatory responses. Future studies should focus on optimizing priming conditions, elucidating the molecular pathways underlying these adaptations, and, once optimized, validating the therapeutic efficacy of these EVs in vivo.

Acknowledgments

The library preparation and sequencing were performed at the DNA Technologies and Expression Analysis Cores at the UC Davis Genome Center, supported by NIH Shared Instrumentation Grant 1S10OD010786-01. We also want to thank Lori Haapanen for her assistance with the Luminex assays.

Author Contributions

M.S.R. conception and design, provision of study material or patients, data analysis and interpretation, manuscript writing. B.A. financial support, data analysis, and interpretation, manuscript writing. L.B. conception and design, collection and assembly of data, data analysis and interpretation, manuscript writing. K.M. conception and design, financial support, data analysis and interpretation, manuscript writing, final approval of manuscript.

All authors contributed to and approved the final version of the manuscript.

Funding

The George and Phyllis Miller Feline Health Trust of the San Francisco Foundation provided financial support for this study, which was administered by the Center for Companion Animal Health, University of California-Davis, through grant number 2022-2-F. The project described was supported by the National

Center for Advancing Translational Sciences, National Institutes of Health, through grant number UL1 TR001860. The content is solely the responsibility of the authors and does not necessarily represent the official views of the NIH.

Conflict of Interest

The authors have nothing to disclose.

Data Availability

The data that support the findings of this study are available from the corresponding author upon reasonable request.

References

1. Arzi B, Peralta S, Fiani N, et al. A multicenter experience using adipose-derived mesenchymal stem cell therapy for cats with chronic, non-responsive gingivostomatitis. *Stem Cell Res Ther.* 2020;11:115. https://doi.org/10.1186/s13287-020-01623-9
2. Arzi B, Clark KC, Sundaram A, et al. Therapeutic efficacy of fresh, allogeneic mesenchymal stem cells for severe refractory feline chronic gingivostomatitis. *Stem Cells Transl Med*. 2017;6:1710-1722. https://doi.org/10.1002/sctm.17-0035
3. Arzi B, Mills-Ko E, Verstraete FJM, et al. Therapeutic efficacy of fresh, autologous mesenchymal stem cells for severe refractory gingivostomatitis in cats. *Stem Cells Transl Med*. 2016;5:75-86. https://doi.org/10.5966/sctm.2015-0127
4. Soltero-Rivera M, Hart S, Blandino A, Vapniarsky N, Arzi B. Mesenchymal stromal cell therapy for feline chronic gingivostomatitis: long term experience. *Front Vet Sci*. 2023;10:1171922. https://doi.org/10.3389/fvets.2023.1171922
5. Febre M, Saulnier N, Roux P, et al. Placenta-derived mesenchymal stromal cells as a treatment for refractory chronic gingivostomatitis in cats: eight cases (2018). *J Small Anim Pract*. 2023;64:296-305. https://doi.org/10.1111/jsap.13583
6. Neurath N, Kesting M. Cytokines in gingivitis and periodontitis: from pathogenesis to therapeutic targets. *Front Immunol*. 2024;15:1435054. https://doi.org/10.3389/fimmu.2024.1435054
7. Ma H, Wu Y, Yang H, et al. MicroRNAs in oral lichen planus and potential miRNA-mRNA pathogenesis with essential cytokines: a review. *Oral Surg Oral Medi Oral Pathol Oral Radiol*. 2016;122:164-173. https://doi.org/10.1016/j.oooo.2016.03.018
8. Arzi B, Kol A, Murphy B, et al. Feline foamy virus adversely affects feline mesenchymal stem cell culture and expansion: implications for animal model development. *Stem Cells Dev*. 2015;24:814-823. https://doi.org/10.1089/scd.2014.0317
9. Soltero-Rivera M, Arzi B, Bourebaba L, Marycz K. Distinctive characteristics of extracellular vesicles from feline adipose and placenta stromal cells unveil potential for regenerative medicine in cats. *J Am Vet Med Assoc*. 2024;262:S31-S39. https://doi.org/10.2460/javma.23.11.0662
10. Peralta S, Grenier JK, Webb SM, et al. Transcriptomic signatures of feline chronic gingivostomatitis are influenced by upregulated IL6. *Sci Rep*. 2023;13:13437. https://doi.org/10.1038/s41598-023-40679-4
11. Dolieslager SMJ, Lappin DF, Bennett D, et al. The influence of oral bacteria on tissue levels of Toll-like receptor and cytokine mRNAs in feline chronic gingivostomatitis and oral health. *Vet Immunol Immunopathol*. 2013;151:263-274. https://doi.org/10.1016/j.vetimm.2012.11.016
12. Diehl S, Rincón M. The two faces of IL-6 on Th1/Th2 differentiation. *Mol Immunol*. 2002;39:531-536. https://doi.org/10.1016/s0161-5890(02)00210-9
13. Hirano T, Yasukawa K, Harada H, et al. Complementary DNA for a novel human interleukin (BSF-2) that induces B lymphocytes to produce immunoglobulin. *Nature*. 1986;324:73-76. https://doi.org/10.1038/324073a0
14. Dinarello CA. Immunological and inflammatory functions of the interleukin-1 family. *Annu Rev Immunol*. 2009;27:519-550. https://doi.org/10.1146/annurev.immunol.021908.132612
15. Bradley JR. TNF-mediated inflammatory disease. *J Pathol*. 2008;214:149-160. https://doi.org/10.1002/path.2287
16. Zelová H, Hošek J. TNF-α signalling and inflammation: interactions between old acquaintances. *Inflam Res*. 2013;62:641-651. https://doi.org/10.1007/s00011-013-0633-0
17. Hackel A, Vollmer S, Bruderek K, Lang S, Brandau S. Immunological priming of mesenchymal stromal/stem cells and their extracellular vesicles augments their therapeutic benefits in experimental graft-versus-host disease via engagement of PD-1 ligands. *Front Immunol*. 2023;14:1078551. https://doi.org/10.3389/fimmu.2023.1078551
18. de Noronha NC, Mizukami A, Caliári-Oliveira C, et al. Priming approaches to improve the efficacy of mesenchymal stromal cell-based therapies. *Stem Cell Res Ther*. 2019;10:131. https://doi.org/10.1186/s13287-019-1224-y
19. Nava MM, Raimondi MT, Pietrabissa R. Controlling self-renewal and differentiation of stem cells via mechanical cues. *J Biomed Biotechnol*. 2012;2012:797410. https://doi.org/10.1155/2012/797410
20. Huang C, Dai J, Zhang XA. Environmental physical cues determine the lineage specification of mesenchymal stem cells. *Biochim Biophys Acta*. 2015;1850:1261-1266. https://doi.org/10.1016/j.bbagen.2015.02.011
21. Zhou Y, Tsai T-L, Li W-J. Strategies to retain properties of bone marrow-derived mesenchymal stem cells ex vivo. *Ann N Y Acad Sci*. 2017;1409:3-17. https://doi.org/10.1111/nyas.13451
22. Baldari S, Di Rocco G, Piccoli M, et al. Challenges and strategies for improving the regenerative effects of mesenchymal stromal cell-based therapies. *Int J Mol Sci*. 2017;18:2087. https://doi.org/10.3390/ijms18102087
23. Petrenko Y, Syková E, Kubinová S. The therapeutic potential of three-dimensional multipotent mesenchymal stromal cell spheroids. *Stem Cell Res Ther*. 2017;8:94. https://doi.org/10.1186/s13287-017-0558-6
24. Hu C, Li L. "Preconditioning influences mesenchymal stem cell properties in vitro and in vivo.". *J Cell Mol Med*. 2018;22:1428-1442. https://doi.org/10.1111/jcmm.13492
25. Prasanna SJ, Gopalakrishnan D, Shankar SR, Vasandan AB. Pro-inflammatory cytokines, IFNgamma and TNFalpha, influence immune properties of human bone marrow and Wharton jelly mesenchymal stem cells differentially. *PLoS One*. 2010;5:e9016. https://doi.org/10.1371/journal.pone.0009016
26. François M, et al. "Human MSC suppression correlates with cytokine induction of indoleamine 2,3-dioxygenase and bystander M2 macrophage differentiation.". *Mol Ther*. 2012;20:187-195. https://doi.org/10.1038/mt.2011.189
27. Carrero R, Cerrada I, Lledó E, et al. "IL1β induces mesenchymal stem cells migration and leucocyte chemotaxis through NF-κB.". *Stem Cell Rev Rep*. 2012;8:905-916. https://doi.org/10.1007/s12015-012-9364-9
28. Fan H, Zhao G, Liu L, et al. "Pre-treatment with IL-1β enhances the efficacy of MSC transplantation in DSS-induced colitis.". *Cellular Mol Immunol*. 2012;9:473-481. https://doi.org/10.1038/cmi.2012.40
29. Clemente-Suárez VJ, Martín-Rodríguez A, Yáñez-Sepúlveda R, Tornero-Aguilera JF. Mitochondrial transfer as a novel therapeutic approach in disease diagnosis and treatment. *Int J Mol Sci* . 2023;24:8848. https://doi.org/10.3390/ijms24108848
30. Murray LMA, Krasnodembskaya AD. Concise review: intercellular communication via organelle transfer in the biology and therapeutic applications of stem cells. *Stem Cells*. 2019;37:14-25. https://doi.org/10.1002/stem.2922
31. Spees JL, Olson SD, Whitney MJ, Prockop DJ. Mitochondrial transfer between cells can rescue aerobic respiration. *Proc Natl*

Acad Sci USA. 2006;103:1283-1288. https://doi.org/10.1073/pnas.0510511103
32. Islam MN, Das SR, Emin MT, et al. "Mitochondrial transfer from bone-marrow-derived stromal cells to pulmonary alveoli protects against acute lung injury.". *Nat Med*. 2012;18:759-765. https://doi.org/10.1038/nm.2736
33. Hayakawa K, Chan SJ, Mandeville ET, et al. Protective effects of endothelial progenitor cell-derived extracellular mitochondria in brain endothelium. *Stem Cells*. 2018;36:1404-1410. https://doi.org/10.1002/stem.2856
34. Zhang T-G, Miao C-Y. "Mitochondrial transplantation as a promising therapy for mitochondrial diseases.". *Acta Pharmaceutica Sinica. B* 2023;13:1028-1035. https://doi.org/10.1016/j.apsb.2022.10.008
35. Js B, Gk B, Ph R. Mitochondrial dysfunction and oxidative stress in metabolic disorders - A step towards mitochondria based therapeutic strategies. *Biochim Biophys Acta Mol Basis Dis*. 2017;1863:1066. https://doi.org/10.1016/j.bbadis.2016.11.010
36. Soltero-Rivera M, Groborz S, Janeczek M, et al. Gingiva-derived stromal cells isolated from cats affected with tooth resorption exhibit increased apoptosis, inflammation, and oxidative stress while experiencing deteriorated expansion and anti-oxidative defense. *Stem Cell Rev Rep*. 2023;19:1507-1523. https://doi.org/10.1007/s12015-023-10537-x
37. Lavrentieva A, Majore I, Kasper C, et al. Effects of hypoxic culture conditions on umbilical cord-derived human mesenchymal stem cells. *Cell Commun Signal*. 2010;8:1. https://doi.org/10.1186/1478-811X-8-18
38. Surma M, Anbarasu K, Dutta S, et al. Enhanced mitochondrial biogenesis promotes neuroprotection in human pluripotent stem cell derived retinal ganglion cells. *Commun Biol*. 2023;6:218. https://doi.org/10.1038/s42003-023-04576-w
39. Mukkala AN, Jerkic M, Khan Z, et al. Therapeutic effects of mesenchymal stromal cells require mitochondrial transfer and quality control. *Int J Mol Sci* . 2023;24:15788. https://doi.org/10.3390/ijms242115788
40. Hong T, Kim MY, Da Ly D, et al. Ca2+-activated mitochondrial biogenesis and functions improve stem cell fate in Rg3-treated human mesenchymal stem cells. *Stem Cell Res Ther*. 2020;11:467. https://doi.org/10.1186/s13287-020-01974-3
41. Chen W, Zhao H, Li Y. Mitochondrial dynamics in health and disease: mechanisms and potential targets. *Signal Transd Targeted Ther*. 2023;8:1-25. https://doi.org/10.1038/s41392-023-01547-9
42. López-García L, Castro-Manrreza ME. TNF-α and IFN-γ participate in improving the immunoregulatory capacity of mesenchymal stem/stromal cells: importance of cell–cell contact and extracellular vesicles. *Int J Mol Sci*. 2021;22:9531. https://doi.org/10.3390/ijms22179531
43. DelaRosa O, Lombardo E, Beraza A, et al. Requirement of IFN-gamma-mediated indoleamine 2,3-dioxygenase expression in the modulation of lymphocyte proliferation by human adipose-derived stem cells. *Tissue Eng Part A*. 2009;15:2795-2806. https://doi.org/10.1089/ten.TEA.2008.0630
44. Cheng A, Choi D, Lora M, et al. Human multipotent mesenchymal stromal cells cytokine priming promotes RAB27B-regulated secretion of small extracellular vesicles with immunomodulatory cargo. *Stem Cell Res Ther*. 2020;11:539. https://doi.org/10.1186/s13287-020-02050-6
45. Sokolova V, Ludwig A-K, Hornung S, et al. Characterisation of exosomes derived from human cells by nanoparticle tracking analysis and scanning electron microscopy. *Colloids Surf B*. 2011;87:146-150. https://doi.org/10.1016/j.colsurfb.2011.05.013
46. Peng J-Y, Lin C-C, Chen Y-J, et al. Automatic morphological subtyping reveals new roles of caspases in mitochondrial dynamics. *PLoS Comput Biol*. 2011;7:e1002212. https://doi.org/10.1371/journal.pcbi.1002212
47. Bang Y, Hwang S, Kim YE, et al. Therapeutic efficacy of thrombin-preconditioned mesenchymal stromal cell-derived extracellular vesicles on Escherichia coli-induced acute lung injury in mice. *Respir Res*. 2024;25:303. https://doi.org/10.1186/s12931-024-02908-w
48. Park SM, Oh YH, Lim GH, et al. Deferoxamine preconditioning of canine stem cell derived extracellular vesicles alleviates inflammation in an EAE mouse model through STAT3 regulation. *Sci Rep*. 2024;14:19273. https://doi.org/10.1038/s41598-024-68853-2
49. Sung DK, Sung SI, Ahn SY, Chang YS, Park WS. Thrombin preconditioning boosts biogenesis of extracellular vesicles from mesenchymal stem cells and enriches their cargo contents via protease-activated receptor-mediated signaling pathways. *Int J Mol Sci*. 2019;20:2899. https://doi.org/10.3390/ijms20122899
50. Sung DK, Chang YS, Sung SI, et al. Antibacterial effect of mesenchymal stem cells against Escherichia coli is mediated by secretion of beta- defensin- 2 via toll- like receptor 4 signalling. *Cell Microbiol*. 2016;18:424-436. https://doi.org/10.1111/cmi.12522
51. Allen H, Shraga-Heled N, Blumenfeld M, et al. Human placental-derived adherent stromal cells co-induced with TNF-α and IFN-γ inhibit triple-negative breast cancer in nude mouse xenograft models. *Sci Rep*. 2018;8:670. https://doi.org/10.1038/s41598-017-18428-1
52. Grzelkowska-Kowalczyk K, Wieteska-Skrzeczyńska W. Treatment with TNF-alpha and IFN-gamma alters the activation of SER/THR protein kinases and the metabolic response to IGF-I in mouse c2c12 myogenic cells. *Cell Mol Biol Lett*. 2010;15:13-31. https://doi.org/10.2478/s11658-009-0033-1
53. Eugenín EA, et al. TNF-alpha plus IFN-gamma induce connexin43 expression and formation of gap junctions between human monocytes/macrophages that enhance physiological responses. *J Immunol*. 2003;170:1320-1328. https://doi.org/10.4049/jimmunol.170.3.1320
54. Jin Q-H, Kim H-K, Na J-Y, Jin C, Seon J-K. Anti-inflammatory effects of mesenchymal stem cell-conditioned media inhibited macrophages activation in vitro. *Sci Rep*. 2022;12:4754. https://doi.org/10.1038/s41598-022-08398-4
55. Kang M, Huang C-C, Gajendrareddy P, et al. Extracellular vesicles from TNFα preconditioned MSCs: effects on immunomodulation and bone regeneration. *Front Immunol*. 2022;13:878194. https://doi.org/10.3389/fimmu.2022.878194
56. Harting MT, Srivastava AK, Zhaorigetu S, et al. Inflammation-stimulated mesenchymal stromal cell-derived extracellular vesicles attenuate inflammation. *Stem Cells*. 2018;36:79-90. https://doi.org/10.1002/stem.2730
57. Riccardi C, Nicoletti I. Analysis of apoptosis by propidium iodide staining and flow cytometry. *Nat Protocols*. 2006;1:1458-1461. https://doi.org/10.1038/nprot.2006.238
58. van Niel G, D'Angelo G, Raposo G. Shedding light on the cell biology of extracellular vesicles. *Nat Rev Mol Cell Biol*. 2018;19:213-228. https://doi.org/10.1038/nrm.2017.125
59. Zhang Y, Liu Y, Liu H, Tang WH. Exosomes: biogenesis, biologic function and clinical potential. *Cell Biosci*. 2019;9:19. https://doi.org/10.1186/s13578-019-0282-2
60. Gustafson CM, Shepherd AJ, Miller VM, Jayachandran M. Age- and sex-specific differences in blood-borne microvesicles from apparently healthy humans. *Biol Sex Differ*. 2015;6:10. https://doi.org/10.1186/s13293-015-0028-8
61. Torralba D, Baixauli F, Villarroya-Beltri C, et al. Priming of dendritic cells by DNA-containing extracellular vesicles from activated T cells through antigen-driven contacts. *Nat Commun*. 2018;9:2658. https://doi.org/10.1038/s41467-018-05077-9
62. Eisner V, Picard M, Hajnóczky G. Mitochondrial dynamics in adaptive and maladaptive cellular stress responses. *Nat Cell Biol*. 2018;20:755-765. https://doi.org/10.1038/s41556-018-0133-0
63. Kari S, Subramanian K, Altomonte IA, et al. Programmed cell death detection methods: a systematic review and a categorical comparison. *Apoptosis*. 2022;27:482-508. https://doi.org/10.1007/s10495-022-01735-y
64. Ward TH, Cummings J, Dean E, et al. Biomarkers of apoptosis. *Br J Cancer*. 2008;99:841-846. https://doi.org/10.1038/sj.bjc.6604519

65. Lugini L, Cecchetti S, Huber V, et al. Immune surveillance properties of human NK cell-derived exosomes. *J Immunol*. 2012;189:2833-2842. https://doi.org/10.4049/jimmunol.1101988
66. Zhang J, Li S, Li L, et al. Exosome and exosomal microRNA: trafficking, sorting, and function. *Genomics Proteomics Bioinformatics*. 2015;13:17-24. https://doi.org/10.1016/j.gpb.2015.02.001
67. Phinney DG, Di Giuseppe M, Njah J, et al. Mesenchymal stem cells use extracellular vesicles to outsource mitophagy and shuttle microRNAs. *Nat Commun*. 2015;6:8472. https://doi.org/10.1038/ncomms9472
68. Sansone P, Savini C, Kurelac I, et al. Packaging and transfer of mitochondrial DNA via exosomes regulate escape from dormancy in hormonal therapy-resistant breast cancer. *Proc Natl Acad Sci USA*. 2017;114:E9066-E9075. https://doi.org/10.1073/pnas.1704862114
69. Tomasoni S, Longaretti L, Rota C, et al. Transfer of growth factor receptor mRNA via exosomes unravels the regenerative effect of mesenchymal stem cells. *Stem Cells Dev*. 2013;22:772-780. https://doi.org/10.1089/scd.2012.0266
70. St-Pierre J, Drori S, Uldry M, et al. Suppression of reactive oxygen species and neurodegeneration by the PGC-1 transcriptional coactivators. *Cell*. 2006;127:397-408. https://doi.org/10.1016/j.cell.2006.09.024
71. Dhar SS, Ongwijitwat S, Wong-Riley MTT. Nuclear respiratory factor 1 regulates all ten nuclear-encoded subunits of cytochrome c oxidase in neurons. *J Biol Chem*. 2008;283:3120-3129. https://doi.org/10.1074/jbc.M707587200
72. Picca A, Guerra F, Calvani R, et al. Mitochondrial dysfunction, protein misfolding and neuroinflammation in parkinson's disease: roads to biomarker discovery. *Biomolecules*. 2021;11:1508. https://doi.org/10.3390/biom11101508
73. Kang I, Chu CT, Kaufman BA. The mitochondrial transcription factor TFAM in neurodegeneration: emerging evidence and mechanisms. *FEBS Lett*. 2018;592:793-811. https://doi.org/10.1002/1873-3468.12989
74. Kucej M, Kucejova B, Subramanian R, Chen XJ, Butow RA. Mitochondrial nucleoids undergo remodeling in response to metabolic cues. *J Cell Sci*. 2008;121:1861-1868. https://doi.org/10.1242/jcs.028605
75. Arzi B, Nolta JA, Vapniarsky N. The oromaxillofacial region as a model for a one-health approach in regenerative medicine. *Am J Vet Res*. 2022;83:291-297. https://doi.org/10.2460/ajvr.21.12.0208
76. Williams ZJ, Pezzanite LM, Chow L, Rockow M, Dow SW. Evaluation of stem-cell therapies in companion animal disease models: a concise review (2015-2023). *Stem Cells*. 2024;42:677-705. https://doi.org/10.1093/stmcls/sxae034
77. Tl W, Cb W. Scoping review of the use of mesenchymal stem and stromal cell products in cats, Part 2: current scope and efficacy. *J Am Vet Med Assoc*. 2024;262(S1):S24. https://doi.org/10.2460/javma.24.02.0080
78. Spaggiari GM, Capobianco A, Becchetti S, Mingari MC, Moretta L. Mesenchymal stem cell-natural killer cell interactions: evidence that activated NK cells are capable of killing MSCs, whereas MSCs can inhibit IL-2-induced NK-cell proliferation. *Blood*. 2006;107:1484-1490. https://doi.org/10.1182/blood-2005-07-2775
79. Herger N, Heggli I, Mengis T, et al. Impacts of priming on distinct immunosuppressive mechanisms of mesenchymal stromal cells under translationally relevant conditions. *Stem Cell Res Ther*. 2024;15:65. https://doi.org/10.1186/s13287-024-03677-5
80. Tappenbeck N, Schröder HM, Niebergall-Roth E, et al. In vivo safety profile and biodistribution of GMP-manufactured human skin-derived ABCB5-positive mesenchymal stromal cells for use in clinical trials. *Cytotherapy*. 2019;21:546-560. https://doi.org/10.1016/j.jcyt.2018.12.005
81. Guess AJ, Daneault B, Wang R, et al. Safety profile of good manufacturing practice manufactured interferon γ-primed mesenchymal stem/stromal cells for clinical trials. *Stem Cells Transl Med*.. 2017;6:1868-1879. https://doi.org/10.1002/sctm.16-0485